Supplementary Information:
Unveiling the Orbital Texture of 1T-TiTe$_2$ using Intrinsic Linear Dichroism in Multidimensional Photoemission Spectroscopy

Samuel Beaulieu,[1,2,*] Michael Schüler,[3,†] Jakub Schusser,[4,5] Shuo Dong,[2] Tommaso Pincelli,[2] Julian Maklar,[2] Alexander Neef,[2] Friedrich Reinert,[4] Martin Wolf,[2] Laurenz Rettig,[2] Ján Minár,[5,‡] and Ralph Ernstorfer[2,6,§]

[1]*Université de Bordeaux - CNRS - CEA, CELIA, UMR5107, F33405 Talence, France*
[2]*Fritz Haber Institute of the Max Planck Society, Faradayweg 4-6, 14195 Berlin, Germany*
[3]*Stanford Institute for Materials and Energy Sciences (SIMES),*
*SLAC National Accelerator Laboratory, Menlo Park, CA 94025, USA*
[4]*Experimentelle Physik VII and Würzburg-Dresden Cluster of Excellence ct.qmat, Universität Würzburg, Würzburg, Germany*
[5]*New Technologies-Research Center, University of West Bohemia, 30614 Pilsen, Czech Republic*
[6]*Institut für Optik und Atomare Physik, Technische Universität Berlin, 10623 Berlin, Germany*
(Dated: October 13, 2021)

In Supplementary Figure 1, we compare *i*LDAD for bulk and monolayer 1T-TiTe$_2$, calculated using the layer-resolved one-step model of photoemission described in the methods. The obtained *i*LDAD for the bulk and monolayer cases are almost identical. Indeed, the features at both Γ and M/M' points do not change when going from the monolayer case to the bulk limit. This striking observation gives us confidence that we can construct the TB model for a free-standing monolayer of 1T-TiTe$_2$ to get an intuitive picture about the orbital physics governing the emergence of the *i*LDAD.
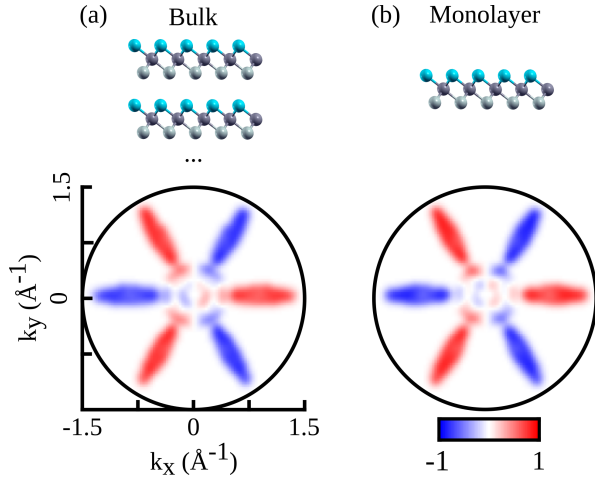
Supplementary Figure 1. **Layer-resolved *i*LDAD calculated within the KKR framework**. *i*LDAD for **(a)** bulk and **(b)** free-standing monolayer of 1T-TiTe$_2$ using 18.7 eV photon energy, and the same parameters as described in the methods.

To probe the bulk *i*LDAD spectrum, we performed corresponding calculations in the soft-x-ray regime. In Supplementary Figure 2 we show photon-energy dependence of the
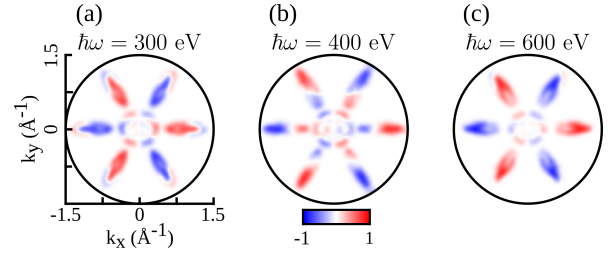
Supplementary Figure 2. **Soft-x-ray *i*LDAD calculated within the KKR framework for different photon energy**. *i*LDAD for bulk 1T-TiTe$_2$ has been calculated in the soft-x-ray regime at different photon energies **(a)** 300 eV, **(b)** 400 eV and **(c)** 600 eV.

*i*LDAD for bulk 1T-TiTe$_2$, for 300 eV, 400 eV and 600 eV photon energies. The photon-energy-dependent trends from the XUV regime (see the main manuscript) are also recovered in the soft-x-ray regime. In particular, the dichroic features around the Γ point reverse sign when increasing the photon energy. However, the observed *i*LDAD at M and M' points, which is stable again variation of photon energy, further support the link between the in-plane orbital texture and *i*LDAD. Furthermore, we point out that by increasing the photon energy to the soft-x-ray regime, TRLEED final states approach free-electron-like character, and the corresponding approximation in the TB model is justified for *i*LDAD features around M and M' points.

Next, we show the procedure to extract the antisymmetric components of the dichroism (referred to as *intrinsic* Linear Dichroism in Photoelectron Angular Distributions - *i*LDAD) from photoemission data obtained from two crystal orientations rotated by 60° with respect to each other, for two different photon energies (18.7 eV and 21.7 eV). These data have been simulated using the one-step model (KKR) described in the manuscript.

* samuel.beaulieu@u-bordeaux.fr
† schuelem@stanford.edu
‡ jminar@ntc.zcu.cz
§ ernstorfer@fhi-berlin.mpg.de
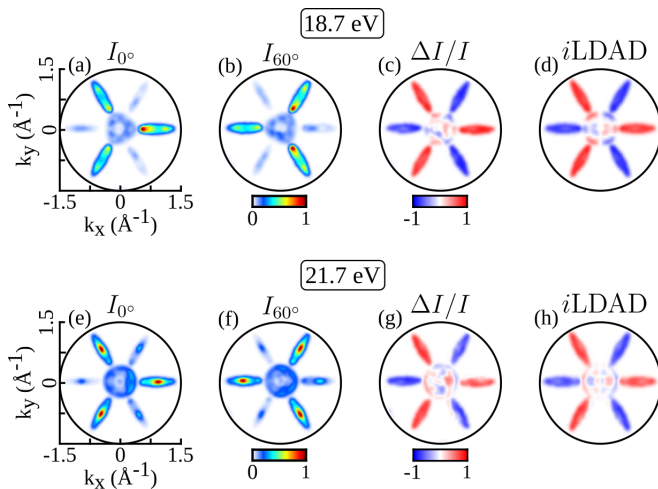
Supplementary Figure 3. **Extraction of the *intrisic* Linear Dichroism in Photoelectron Angular Distributions (*i*LDAD) for different photon energies, calculated using the KKR framework**: **(a)-(b) and (e)-(f)** $I_{0°}$ and $I_{60°}$, the CECs at the Fermi energy, calculated for two crystal orientations rotated by 60° with respect to each others, for 18.7 eV and 21.7 eV photon energies, respectively. **(c) and (g)** $\Delta I/I$, the raw normalized difference, *i.e.* $(I_{0°} - I_{60°})/(I_{0°} + I_{60°})$ between CECs shown in (a)-(b), and (e)-(f), for 18.7 eV and 21.7 eV photon energies, respectively. **(d) and (f)** *i*LDAD represents the component of $A_{LDAD}^{0°/60°}$ (see manuscript for more details) which is antisymmetric upon 60° azimuthal rotation of the crystal, for 18.7 eV and 21.7 eV photon energies, respectively.

As explained in the main text and in the methods section, we have constructed a tight-binding (TB) Hamiltonian based on projective Wannier functions. This procedure yields the Hamiltonian $H_{j,j'}(\mathbf{k})$, where j, j' run over the set of Te-p and Ti-d orbitals (11 orbitals in total). Diagonalizing $H_{j,j'}(\mathbf{k})$ yields the eigenvalues $\varepsilon_n(\mathbf{k})$ and the associated eigenvectors $[\mathbf{C}_n(\mathbf{k})] = C_{jn}(\mathbf{k})$ (which enter Eq. (4), Eq. (6) and Eq. (9) in the main text).

The TB Hamiltonian is particularly useful for projecting onto specific orbitals. We define the orbital weight $w_{jn}(\mathbf{k}) = |C_{jn}(\mathbf{k})|^2$. Fig. (5) in the main text shows the orbital weight for $j \in \{d_{z^2}, d_{xz}, d_{yz}\}$. The Te-$p$ orbitals play only a minor role at the M/M' pockets at the Fermi energy, which is confirmed by Supplementary Figure 4(b). Contrasting the two paths in the Brillouin zone sketched in Fig/ 4(a), we not that the weight of the p_z orbitals is constant, while the p_x orbital has no contribution at M/M' for the path parallel to k_x. The weight of the p_y orbital changes only slightly when considering the rotated path.

Refs. [1, 2] attempted to explain the observed anisotropies in ARPES from the related compounds 1T-TaSe$_2$ and 1T-TaS$_2$ to a crystal-field splitting effect. We used the experimental geometry of the bulk system for all calculations, defined by the lattice constant $a = 3.75$ Å and the vertical distance between the Te layers of $d_{\text{Te}} = 3.367$ Å. In this geometry the crystal axes defined by the Ti-Te bonds, are non-orthogonal. Hence, the angular momentum is quenched, and the Ti-d orbitals in the lab frame would be expressed by orbitals with different total angular momentum in the crystal-field basis. However, for a qualitative picture from the crystal-field point of view, we define the crystal-field axes in a modified geometry where bond directions are orthogonal (see Supplementary Figure 4(c)). This is achieved by reducing the Te layer distance to $d'_{\text{Te}} = 3.054$ Å. The resulting ligand configuration is identical to the octahedral complex; the d orbitals split into the e_g orbitals ($d_{z^2}, d_{x^2-y^2}$) and t_{2g} orbitals (d_{xy}, d_{xz}, d_{yz}) in the new coordinate system (x', y', z').

Inspecting the orbital weight in the crystal-field basis of Ti-d orbitals (Supplementary Figure 4(d)) we find a qualitative difference between e_g and t_{2g} orbitals. The weight of the t_{2g} at the M/M' pockets is almost unchanged when rotating the path in momentum space by 60°, while the e_g orbitals are strongly affected. For the path parallel to the k_x direction (upper panels in Supplementary Figure 4(d)), the $d_{x^2-y^2}$ orbital dominates, while for the rotated path the $d_{x^2-y^2}$ transfers most of its weight to d_{z^2}. This analogous to the exchange of orbital weight between d_{xz} and d_{yz} orbitals in the lab frame discussed in the main text. The analysis in the crystal-field basis provides a complementary but ultimately not simpler picture, as the Bloch wavefunction contains notable contributions from both the e_g and t_{2g} orbitals.

[1] M. M. Traum, N. V. Smith, F. J. Di Salvo, Angular dependence of photoemission and atomic orbitals in the layer compound 1T − TaSe$_2$. *Phys. Rev. Lett.* **32**, 1241–1244 (1974).

[2] N. V. Smith, M. M. Traum, Angular-resolved ultraviolet photoemission spectroscopy and its application to the layer compounds TaSe$_2$ and TaS$_2$. *Phys. Rev. B* **11**, 2087–2108 (1975).
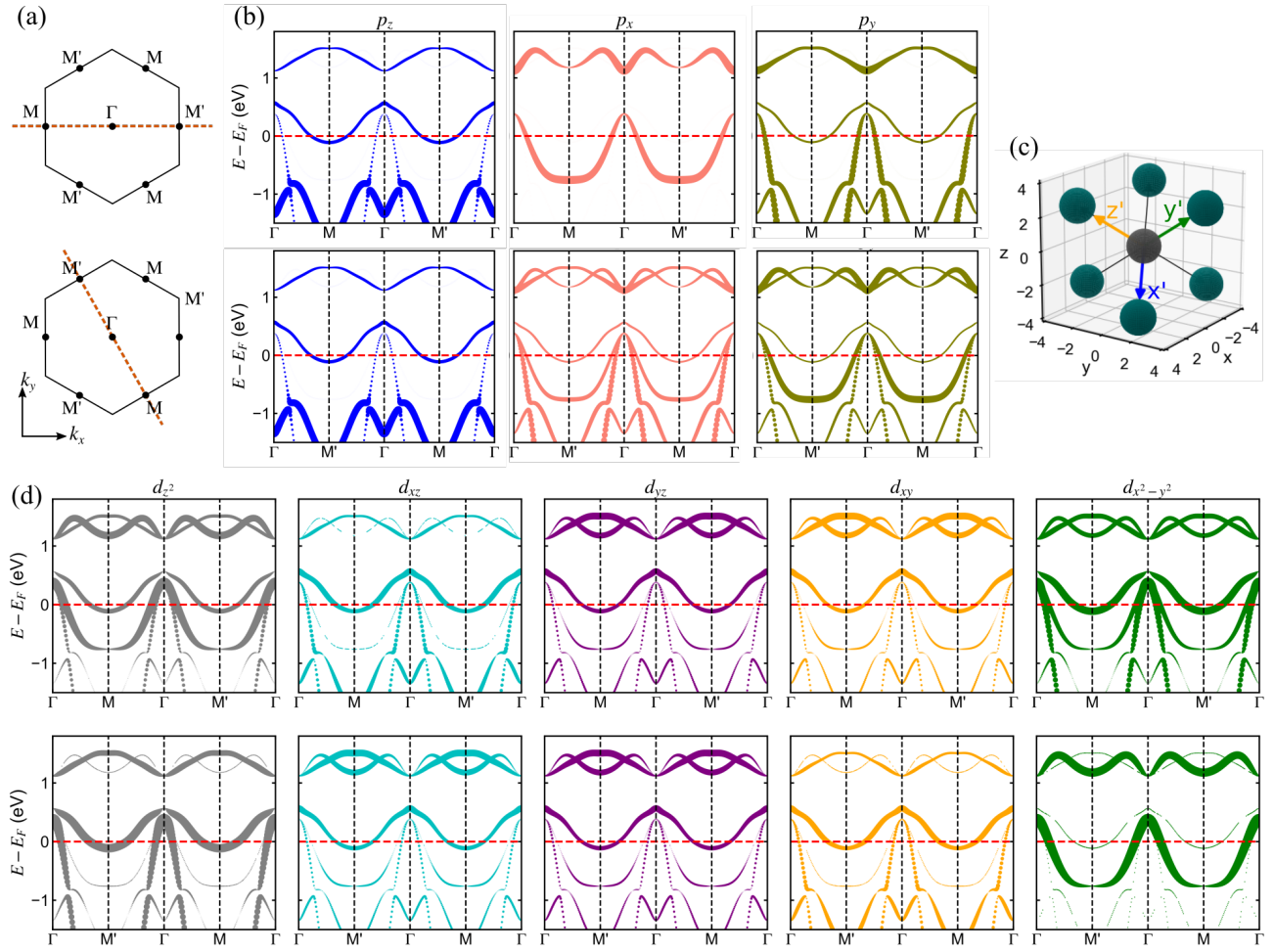
Supplementary Figure 4. **Orbital-projected band structure of monolayer 1T-TiTe$_2$.** **(a)** Sketch of the first Brillouin zone the paths in momentum space along which the band structures have been calculated. **(b)** Analogous to Fig. (5) in the main text, the top (bottom) panels show the fat-band representation of the band structure along the path indicated in the top (bottom) in **(a)**. The thickness represents the summed weight from both Te atoms in the unit cell. The scale of the thickness is identical to Fig. (5) in the main text. **(c)** Sketch of the modified geometry for defining the crystal-field coordinate system (x', y', z'). **(d)** Fat-band representation of the band structure (analogous to **(b)**) in the crystal-field basis.